Liquid Waveguide Cladding for 2D Beam Steering of An Optical Phased Array at a Single Wavelength

Binghui Li [1,2], Caiming Sun [1,3,*], and Aidong Zhang [1,3]
[1]Shenzhen Institute of Artificial Intelligence and Robotics for Society (AIRS), The Chinese University of Hong Kong (CUHK), Shenzhen, China
[2]University of Science and Technology of China, Hefei, Anhui, 230026, China
[3]Robotics Research Center, Peng Cheng Laboratory (PCL), Shenzhen 518055, Guangdong, China
**Author e-mail addressr: cmsun@cuhk.edu.cn*

Abstract: We present the replacing of waveguide liquid claddings to implement 2D beam steering of an optical phased array. A maximum steering angle of >10° was achieved with RI from 1.0 to 1.63 at 940 nm.

1. Introduction

Integrated optical phased arrays (OPAs) provide a robust and on-chip approach to implement two-dimensional (2D) beam steering, which enables an attractive candidate in LiDAR and free-space optical communications [1,2]. Most of 1D waveguide OPAs facilitate the 2D beam steering, on one side, via the tuning of the input light wavelength [3], and on the other, by the control of phase retardations [4]. This wavelength-tuning scheme, however, desires a tunable laser source, raises the manufacturing complexity and may lead to failure upon the wavelength-dependent components. To implement the single-wavelength beam steering, a few methods have been proposed mainly on the longitudinal beam radiation angle of the OPA. These include, but are not limited to, liquid crystal assisted Bragg-reflector outcoupler [5], single OPA with parallel-installed antenna elements [6], OPA incorporation of lens systems [7], or thermo-tuning of the waveguide effective index [8]. These solutions, however, either desire complex nano fabrications, emerge blind spots upon the field of views (FOVs), or entail giant power consumption as well as the temperature shift, which may damage the optical components affiliated on the OPA chip.

Herein, in this Letter, we report a simple liquid-cladded OPA platform to implement the single-wavelength beam steering upon its longitudinal emission angle. The emission angle was steered by tuning of the waveguide mode effective index n_{eff}. However, this approach for modifying n_{eff} will be more straightforward, i.e., by replacing the liquid claddings in the OPA grating antenna region. To enable the beam steering, the waveguide cladding in antenna region will be fully etched and replaced by the refractive index liquids. This induces the change of waveguide effective index Δn_{eff}, and thus leading to steering of the OPA longitudinal emission angle. Due to high index range of the liquids from the air to ~1.8, the liquid-cladded OPA platform ensures a large n_{eff} tuning range. Compared to conventional optical modulations, such as electro-optic or acousto-optic, the liquid/fluidic steering reveals much larger index modification range at the order of ~1, while others normally weak in insufficient index tuning range of <0.1. Moreover, compared to the indirect beam steering such as thermo-optic control of n_{eff}, the liquid steering features in low power consumption, and no temperature variation exist on the OPA chip.

2. OPA Design and Methodology

We employ the strip waveguide grating antenna design, in order to obtain a large tunability of n_{eff}. The waveguide upper claddings were replaced from the air (n_L=1.0) to a high refractive index (RI, n_L ~1.63 in this work). Based on a prototype of 32-channel silicon nitride OPA, we demonstrated the beam steering range of ~6.1° ~8.4° and 10.1° for the wavelength of λ=785 nm, 852 nm and 940 nm, respectively. Moreover, the liquid-cladded OPA reveals a quasi-continuous beam steering range of >29° by combining liquid cladding tuning and discrete wavelength tuning of λ=785 nm, 852 nm and 940 nm. Figure 1(a) illustrates the schematic diagram of the proposed liquid-cladded OPA layout. The OPA consists of an edge coupler with inverse taper design, 5 stages of 1×2 multimode interference (MMI) splitter trees and 32 channels of waveguide grating antenna (WGA) arrays. The fabrication of OPA chip was performed in the Interuniversity Micro Electronics Center (IMEC) based on a standard CMOS foundry technique. The thickness of buried oxide (BOX) layer and the silicon nitride core layer were 3.3 μm and h=300 nm, respectively. The grating antenna was fully etched at the sides of silicon nitride core (width w=0.55 μm). Figures 1(b) shows the top view of fabricated two OPAs, wherein one OPA was cladded in the antenna region (grey) and another was uncladded (light blue). Figures 1(c)-1(d) illustrates the SEM images of the apodized grating antennas in the uncladded OPA. The OPA array features of grating array period d~4.5 μm. The total aperture size of OPA antenna was quasi-square shaped of ~146 ×144 μm^2.

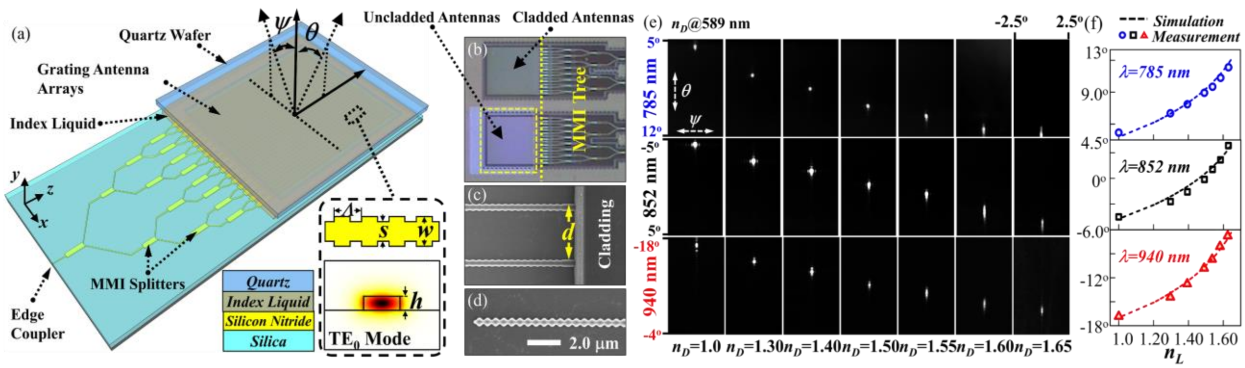

Fig. 1. (a) Schematic diagram of liquid-cladded OPA beam steering platform; (b) Microscopic top-view of cladded and uncladded OPA layouts; (c) SEM image of uncladded OPA antenna regions; (d) the magnified waveguide grating antennas; (e) The captured shift of far-field patterns of OPA at different working wavelength; and (e) The comparison of measurement and simulation beam steering ranges at the respective light wavelength.

To hold the liquid inside the grating antennas, a quartz wafer was carefully positioned on top of the grating antennas at ~100 μm by a micro-positioner. Thereby, a liquid cavity was formed between the uncladded OPA antennas and the quartz wafer, as shown in Figure 1(a). The index liquids were then dropped onto the cavity edge, further absorbed into cavity by the capillary attraction force, and finally functioned as stable claddings for OPA antennas. We use the commercial software Lumerical FDTD solutions for theoretical prediction of the beam steering angle θ versus the RI of the liquid claddings n_L. Firstly, we obtained the waveguide effective indices n_{eff} under different liquid claddings n_L by theoretical simulations. After that, the steering of longitudinal emission angle θ were calculated by referring to the grating diffraction equation $\sin\theta = n_{eff} - \lambda/\Lambda$. For comparison, three wavelengths of λ=785 nm, 852 nm, 940 nm were selected for both theoretical predictions and experimental characterizations. The selected refractive index liquids (Cargille Laboratories) claim the RI range from n_D=1.0 to n_D =1.65. Here n_D represents the RI of liquids at a specified wavelength of λ=589 nm, while the liquid RI n_L should be re-calculated with respect to the working wavelength.

3. Results and Discussions

The measured far-field projections of liquid-cladded OPA were depicted in Figure 1(e) at λ=785 nm, 852 nm and 940 nm, respectively. All the far-field projections indicate circular patterns at low n_L ranges; however, the patterns were slightly broadened at high n_L ranges. This is the intrinsic property of the apodized deisign of the OPA antennas. Figure 1(e) reveals that the longitudinal emission angles θ intend to increase by adopting high-RI liquids as the waveguide claddings. However, the array angles ψ remain unchanged throughout the measurement. This trend follows well with the grating equation. Figure 1(f) plots the measured beam emission angle θ versus the liquids RI from n_D =1.0 to n_D =1.65, at λ=785 nm (blue), 852 nm (black) and 940 nm (red), respectively. The dotted lines refer to the theoretical calculation of θ, while the scatters denote the measured experimental results. These two data fit well with each other with slight differences. To quantify, the results in Figure 1(f) reveal that the beam steering ranges of emission angles θ were ~6.1°, ~8.4° and ~10.1°, for λ=785 nm, 852 nm and 940 nm, respectively. This wavelength dependency of steering range is mainly from the wavelength dependency of mode effective index change Δn_{eff} with the liquid RI n_L. For n_D =1.65(n_L ~1.631) at λ=785 nm, the waveguide mode remains well confined; however, the waveguide mode tends to be weakly guided for n_D =1.65 (n_L~1.625) at λ=940 nm. Therefore, the mode effective index Δn_{eff} changes more abruptly for λ=940 nm, which leads to a larger steering range of θ in this case.

By combination of wavelength tuning and liquid cladding tuning, the result in Figure 1(f) reveals a quasi-continuous beam steering range of >29° (from -17° to 12°). This result claims the excellent scalability of liquid-cladded OPA to integrate the on-chip wavelength-tuning scheme, in order to facilitate the wide-angle beam steering based on a single OPA chip. For comparison, the liquid-cladded OPA performs greater beam steering ranges versus the thermo-optic tuning based OPA design [8]. However, the liquid-cladded OPA employs advantages of non-temperature variations and potentially low-power-consumptions by integration with optofluidic systems.

We also investigated other characteristics, including the beam divergence angle ψ_{FWHM} and 2nd order of grating lobes, as shown in Figure 2(a). The position of 2nd order grating lobes can be calculated by the equation: $\psi' = \pm \sin\text{-}1(\lambda/d)$. To simplify, we only plot the measured profile in the case of n_D =1.50 for λ=785 nm, 852 nm and 940 nm, respectively. The measured peak positions of the λ order grating lobes are well consistent with the theoretical calculations. The minor differences of <0.2º was mainly due to the measurement precision. The beam divergence angles ψ_{FWHM} of the main lobes were estimated as 0.29º, 0.32º, 0.36º, for λ=785 nm, 852 nm and 940 nm, respectively. These values match closely with theoretical predictions of 0.276º, 0.30º and 0.331º based on the equation $\psi_{FWHM}\approx 0.886\lambda/Nd\cos\psi$, where N, d, ψ denotes the waveguide array number, array period and array angle, respectively. The inset in Figure 2(a) shows an example of near-field pattern for the liquid-cladded OPA at λ=852 nm and n_D =1.50 (n_L~1.491 at λ=852 nm). Uniform beam emission can be observed in both θ and ψ directions. This uniform emission is of great help to ensure the circular far-field patterns and low beam divergence angles.

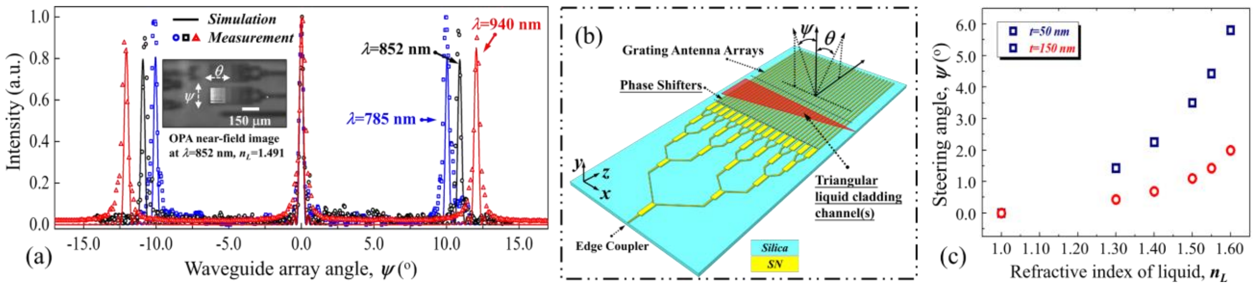

Fig. 2. (a) Measured (colored scatters) characteristics and theoretical (solid lines) predictions of liquid cladded OPA platform; (b) Schematic diagram of transverse OPA beam steering via single or multiple liquid cladding channels; (c) Simulated transverse steering angle versus the liquid cladding index at different residual silica layer thickness.

In addition, the liquid-steering principle applies equally to the transversal beam radiation angle ψ, so as to realize all-fluidic 2D beam steering. This can be done by designing a single or multiple triangular liquid channels to introduce a phase gradient on the OPA phase shifting region, as shown in Fig. 2(b). The triangular channels can be fabricated by physical etching of waveguide upper cladding with a residual silica layer thickness of t. We present the simulation result of transverse beam steering angle ψ versus the liquid refractive index n_L. The residual thickness of t=50 nm and t=150 nm was compared in Fig. 2(c), wherein the result indicates a better beam steering range by deeper etching of residual layers. In addition, the beam steering range can achieve up to ~6º at n_L ~1.60 by a single liquid channel. This range can be further improved by design of multiple liquid channels.

4. Conclusion

In conclusion, we propose a new scheme of liquid-cladded OPA platform for single-wavelength beam steering upon the longitudinal emission angle. The beam steering was realized by replacing the liquid claddings of the waveguide in the grating antenna region. A maximum steering angle of ~10.1º was achieved with a RI range from the air to n_L =1.625 at λ=940nm. Further efficiency improvement and integration with optofluidic systems offer the OPA of all-fluidic 2D beam steering at a single wavelength.

5. Funding:

National Natural Science Foundation of China (NSFC 62105275, 62175120, U1813207); Shenzhen Fundamental Research and Discipline Layout project (JCYJ20180508163015880); Guangdong Special Support Plan (2019TQ05X062).

6. Reference

[1] C. V. Poulton, M. J. Byrd, P. Russo, E. Timurdogan, M. Khandaker, D. Vermeulen, and M. R. Watts, "Long-range LiDAR and free-space data communication with high-performance optical phased arrays." IEEE J. Sel. Top. Quantum Electron. **25**, 1-8 (2019).
[2] B. Li, C. Sun, H. Wang, Z. Chen, X. Nie, S. Deng, L. Yang, A. Zhang, "Liquid-cladded optical phased array for a single-wavelength beam steering," Optics Letters **46**, 4948-4951 (2021).).
[3] H. Wang, Z. Chen, C. Sun, S. Deng, X. Tang, L. Zhang, R. Jiang, W. Shi, Z. Chen, Z. Li, and A. Zhang, "Broadband silicon nitride nanophotonic phased arrays for wide-angle beam steering." Opt. Lett. **46**, 286-289 (2021).
[4] D. N. Hutchison, J. Sun, J. K. Doylend, R. Kumar, J. Heck, W. Kim, C. T. Phare, A. Feshali, and H. Rong. "High-resolution aliasing-free optical beam steering." Optica, **3**, 887-890 (2016).
[5] K. Nakamura, K. Narumi, K. Kikuchi, and Y. Inada, "Liquid-crystal tunable optical phased array for LiDAR applications." in Smart Photonic and Optoelectronic Integrated Circuits XXIII (International Society for Optics and Photonics, 2021), p. 32.
[6] N. A. Tyler, D. Fowler, S. Malhouitre, S. Garcia, P. Grosse, W. Rabaud, and B. Szelag, "SiN integrated optical phased arrays for two-dimensional beam steering at a single near-infrared wavelength." Opt. Express **27**, 5851-5858 (2019).
[7] C. Li, X. Cao, K. Wu, X. Li, and J. Chen. "Lens-based integrated 2D beam-steering device with defocusing approach and broadband pulse operation for Lidar application." Opt. Express **27**, 32970-32983 (2019).
[8] B. Li, C. Sun, H. Wang, X. Nie, Z. Chen, and A. Zhang, "Integrated Optical Phased Array for Temperature Sensing", Conf. Lasers Electro-Optics (CLEO), paper ATh4Q.2, 9-14 May 2021.